



UNIVERSITY OF LEEDS

This is a repository copy of *Vertical annular flow pattern characterisation using proper orthogonal decomposition of Electrical Impedance Tomography*.

White Rose Research Online URL for this paper:
<http://eprints.whiterose.ac.uk/133558/>

Version: Accepted Version

Article:

Polansky, J and Wang, M (2018) Vertical annular flow pattern characterisation using proper orthogonal decomposition of Electrical Impedance Tomography. *Flow Measurement and Instrumentation*, 62. pp. 281-296. ISSN 0955-5986

<https://doi.org/10.1016/j.flowmeasinst.2018.05.001>

© 2018, Elsevier Ltd. All rights reserved. This is an author produced version of a paper published in *Flow Measurement and Instrumentation*. Uploaded in accordance with the publisher's self-archiving policy.

Reuse

This article is distributed under the terms of the Creative Commons Attribution-NonCommercial-NoDerivs (CC BY-NC-ND) licence. This licence only allows you to download this work and share it with others as long as you credit the authors, but you can't change the article in any way or use it commercially. More information and the full terms of the licence here: <https://creativecommons.org/licenses/>

Takedown

If you consider content in White Rose Research Online to be in breach of UK law, please notify us by emailing eprints@whiterose.ac.uk including the URL of the record and the reason for the withdrawal request.



eprints@whiterose.ac.uk
<https://eprints.whiterose.ac.uk/>

Vertical annular flow pattern characterisation using proper orthogonal decomposition of Electrical Impedance Tomography

Jiri Polansky, Mi Wang

School of chemical and process engineering, University of Leeds, LS2 9JT, UK

Abstract

Annular flow is one of the most important multiphase flow regimes primarily because of its presence in extensive industrial applications, such as steam generators, evaporators, condensers and boiling water reactors. There is a great need to have specific techniques capable of extracting characteristics of annular flow pattern via experiment and/or modelling, which is essential to understand specific annular flow phenomena. The intention of developing a mathematical decomposition method for flow regime recognition comes from the fact that each regime is characterised by unique dynamic behaviour. The direct approach with Proper Orthogonal Decomposition (POD) was previously introduced by Lumley, which required a very large amount of relevant data from experimental multiphase and process conditions is necessary. The presented approach is to apply POD on a large amount of tomograms for identification of annular flow pattern in a gas-liquid two phase flow, which also provides a new method to extend the current evaluation procedure of Electrical Impedance Tomography (EIT) for imaging of air-water pipeline flows. The paper demonstrates the capability of the proposed method with a study on annular flow patterns in vertical pipeline.

Email addresses: jiri.polansky@icloud.com (Jiri Polansky),
m.wang@leeds.ac.uk (Mi Wang)

1. Introduction

1.1. Multiphase flow classification

Gas-liquid flows occur in many industrial contexts, such as mining, pumping, separation and transportation of gas and oil, chemical and pharmaceutical processing [1], power energy systems, especially nuclear industries [2] and so on. Multiphase flows are also a ubiquitous feature of the environment whether one considers rain, snow, fog, avalanches, mud slides, sediment transport and debris flows. Very important biological and medical flows are also multiphase, such as blood flow and aerosol inhalation.

One of the fundamental specifics of multiphase flow patterns is the extent to the separation of components in macro-scale [3]. At the ends of the spectrum of the separation, flow patterns are those termed as disperse or separated components. A disperse flow pattern is as that one of its phases or components in a form of drops, bubbles, or particles is widely distributed in other continuous phase. On the other hand, a separated flow consists of separated components in streams of other continuous phases. Various degrees of component separation exist even within each of these limited states. There are many practical disperse flows, such as bubbly or mist flow in a pipe, in which the flow is quite disperse, the particle size is much smaller than the pipe dimensions but the relative motion between the phases is significant.

The relative distribution of the gas and liquid phases can take many different configurations depending on the process conditions, such as the flow rates of the gas and liquid. The configuration of the gas and liquid phases is known as the flow regime. The flow regime describes the pattern of the inner structure of the flow and important hydrodynamic features such as volume fraction, phase and velocity distributions. Two-phase flow regimes are often determined subjectively using direct methods such as the eyeballing method, high-speed photography method and the radioactive attenuation method. Empirical flow regime maps such as the Baker chart [4] are commonly used for approximation and rapid identification of the flow regime under specific operating conditions. However, due to their approximate and subjective nature, these techniques are not able to identify the prevalent multiphase flow regime with the required degree of accuracy.

1.2. Flow pattern estimation

The prediction of flow patterns for fully developed gas-liquid flows typically employs mechanistic models that use different pressure drop and void

fraction estimation procedures for each flow pattern [5]. Accurate prediction of heat transfer, void fraction and pressure drop in gas-liquid flow is important in the design and optimisation of the unit operations dealing with such systems [6]. Therefore different flow regimes require specific modelling approaches to predict their respective transfer properties [7].

Hence in order to produce a reliable design for a multiphase system it is imperative to be able to accurately determine the prevalent flow regime. In the recognition of the prevalent flow pattern the relative quantities of the phases and the topology of their interfaces must be considered. In two phase flow many flow regimes are possibly presented, such as stratified, bubbly, slug, plug and annular flow regimes among others. The flow regime actively depends on a number of factors: the fluid transport and material properties, flow rates, flow direction (co-current or counter-current), the shape and size of the conduit and the orientation (horizontal or vertical) [8]. Considering the orientation of the flow, due to differences in the densities of the phases, vertical flow patterns are different from those obtained in horizontal flow. An intrinsic difference between the two orientations is that horizontal flow patterns are generally not axial-symmetric. This study focuses on vertical gas-liquid annular flow in cylindrical pipes.

1.3. Introduction to electrical impedance tomography

The goal of EIT [9] is to obtain the impedance distribution in the domain of interest. The impedance distribution is obtained by injecting currents or applying voltages to the domain and measuring voltages or currents via a number of electrodes that are mounted non-intrusively but invasively on the boundary of the domain. A pair of EIT sensors consists of two sets of equally spaced electrodes mounted around the periphery of a circular process vessel, in contact with the process fluids inside the vessel.

1.4. Introduction to POD

The target of POD is to extract the synthetic information, which is fundamental to understand the specific fluid dynamics phenomena [10]. POD decomposes a given fluctuating multiphase flow field into a transformation-system of spatial modes, corresponding to orthogonal temporal coefficients. This basis is optimal in the sense that a truncated series expansion of the data has a smaller mean square truncation error than a representation by any other basis. The POD provides a natural ordering of the spatial modes by measure of their mean square temporal amplitude, such as kinetic energy

in the case of velocity. In conjunction with the Galerkin method a system of ordinary differential equations, called the Galerkin system, can be derived for the temporal evolution of the temporal amplitudes [11].

The main aim of the present study is to apply a method of flow regime characterisation, which is based on POD supplemented by frequency and statistical EIT signal analyses.

2. Approach

2.1. Proper orthogonal decomposition

The schematic diagram of POD concept is illustrated in Figure 1. We recognised two fundamental procedures, the preparatory mode and flow characterisation mode. The preparatory mode consists of the following tasks:

- Provide experimental multiphase flow measurement for specific flow conditions, thermo-physical fluid properties and pipeline inclination;
- Carry out EIT, mass flow rates, viscosity, pressure and temperature data acquisition;
- Carry out conductivity and concentration images reconstruction;
- Obtain concentration images, respectively EIT raw data, POD analyses;
- Collect and store POD modes into POD database;
- Analyse POD modes from theoretical fluid dynamics point of view;
- Analyse the frequency of POD modes, relative error and probability density function;
- Compare with the various flow instability mechanisms et al;
- Couple the results with POD modes and specific flow conditions.

Based on the extensive POD functions database the developed method, flow characterisation mode, could be operated secondly, which is illustrated in Figure 1 and further described in the following tasks:

- Provide multiphase flow measurement under unknown flow conditions;

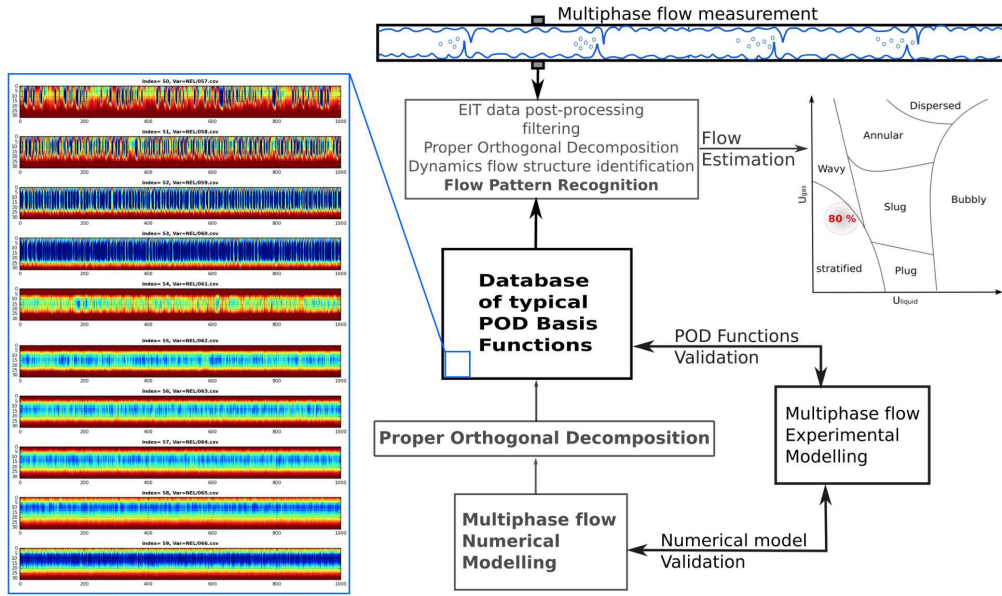


Figure 1: Workflow of POD multiphase flow pattern characterisation

- Carry out EIT data acquisition;
- Input the thermo-physical properties and state of fluid determination (pressure, viscosity, temperature);
- Carry out conductivity and concentration images reconstruction;
- Obtain concentration images, respectively EIT raw data, POD analyses;
- Analyse actual POD modes comparing with POD function database
- Conduct POD modes similarity recognition, flow instability identification, flow conditions, respectively flow patterns characterisation and estimation.

From a mathematical point of view, the Proper Orthogonal Decomposition is a transformation with a diagonal matrix $U(x, t)$ and brings it to a canonical form [12]. The mathematical concept of POD is based on the spectral theory of compact, self adjoints operations. The vector-value function approximation and the conductivity or concentration over the domain of

interest in this study, are supposed as a finite sum in the variables-separated form (1):

$$U(x, t) = \sum_{m=1}^M a_m(x)\phi_m(t), \quad (1)$$

where POD decomposes a given fluctuating conductivity field $U(x, t)$ into an orthogonal normal system of spatial modes $a_m(x)$ and corresponding orthogonal temporal coefficients $\phi_m(t)$. This basis is optimal in the sense that a truncated series expansion of the data in this basis has a smaller mean square truncation error than a representation by any other basis.

The fundamental choices of POD approach are: the input data collection, the inner product, the averaging operation (spatial or temporal) and the variable \vec{X} , where \vec{X} is spatial $\vec{x} = (x, y, z)$ or temporal t . Considering the dimension of process tomography data matrix, it is preferable to use the direct POD approach with the experimental data [13]. In this case the average is temporal, which is evaluated as an ensemble average based on the assumptions of stationary and ergodicity, (see Figure 2). On the other hand, the variable $U(x, t)$ is assimilated to the space variable $x = (x, y, z)$ defined over the domain of interest (two measurement EIT planes each consist of the 360 cells). In order to estimate the set of POD basis functions, Python module Modred 2.0.4 [14] is used. The fundamental characteristics of the procedure are as follow:

- Collect, order and store the conductivity vectors $U = [u_i(x)]$, for each pixels and frame of data acquisition $i = 1, \dots, i_t$.
- Compute each entry of the $i_t \times i_t$ correlation matrix H via $[H]_{i,j} = \langle u_i, u_j \rangle$.
- Compute the eigenvalues and eigenvectors of the correlation matrix, writing $HX = X\Sigma$, where the eigenvalues Σ is diagonal and real, eigenvector X is orthogonal, since H is symmetric.
- Sort the eigenvalues and corresponding eigenvectors in descending order.
- Select the number of modes M , truncate the matrices, keeping first M columns of X to obtain X_M , and first M rows and columns of Σ to obtain Σ_M .

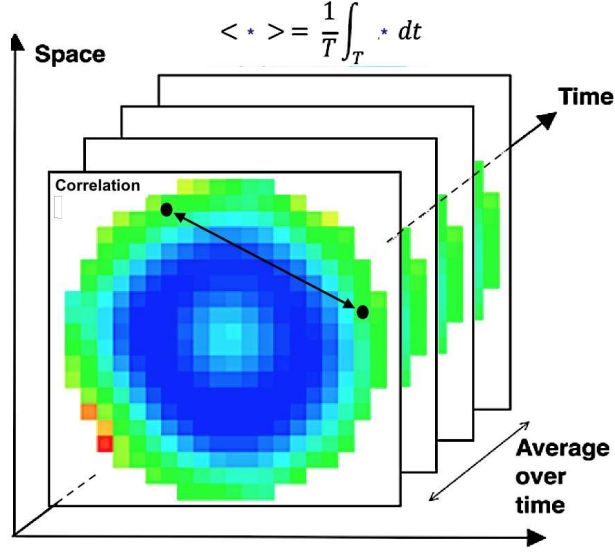


Figure 2: Schematic view of Direct POD approaches

- Compute the matrix of POD modes $A = X_M \Sigma_M^{-1/2}$.
- Construct corresponding temporal coefficients ϕ individually via (2)

$$\phi_m(t) = \sum_{i=1}^{i_t} u_i(x) [A]_{i,m}^T, \quad m = 1, \dots, M. \quad (2)$$

The typical number of modes is $M \in (3 - 20)$. Annular flow reconstruction with relative error below 6% requires approximately five POD modes.

2.2. Gas-liquid test ring

The experiments were carried out in a flow loop built at the University of Leeds with a 3.0 m long, 50 mm internal diameter, transparent, vertical and horizontal working section, which is shown in Figure 3 and described in Table 1.

Air was introduced into the base of the working section via a central tube inside a Y tee. A thermometer was used to provide continuous monitoring of the water temperature. Two differential pressure sensors for measuring the differential pressure drop were placed along the column at around 2.5

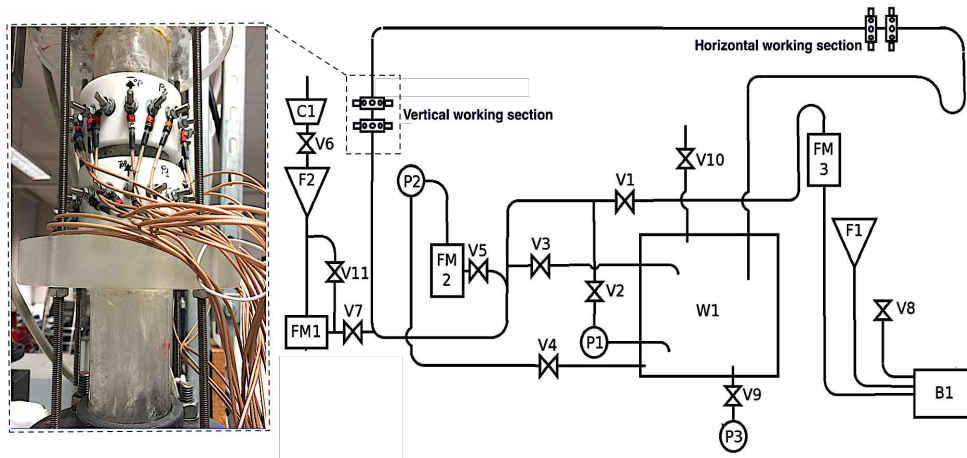


Figure 3: The scheme of updated air-water experimental loop, laboratory of University of Leeds

Table 1: Air-water loop description

Label	Specification	Technical specification	Parameters	Units
V	Valves	manual	-	-
C1	Compressor	Piston	6	Bar
B1	Blower	Centrifugal	150	m^3/h
		max. pressure	30	kPa
W1	Water tank	Open, plastic	200	l
P1	Primary pump	Centrifugal	1	m/s
P2	Secondary pump	Gear	0.15	m/s
FM1	Primary air flow meter	Electromagnetic	50	m^3/h
FM2	Secondary Water flow meter	Rotometer	10	m^3/h
FM3	Secondary air flow meter	Rotometer	130	m^3/h

m above the air distributor. The water volumetric flow rate Q_{water} , varying from 0 to $1.94 \times 10^{-3} m^3/s$ and the primary air volumetric flow rate Q_{air} , varying from 0 to $1.67 \times 10^{-3} m^3/s$ and the secondary air volumetric flow rate Q_{air} , varying from 0 to $3.75 \times 10^{-2} m^3/s$ were measured separately through an electromagnetic flowmeter, and a gas flow controller before they were mixed together. A dual-plane ERT sensor with 16 electrodes per plane was mounted in the inner wall of the pipeline. The electrodes were made of stainless steel with a contact area of 8 mm (width) by 16 mm (height). The data collection rate was 1000 dual-frames/s with an excitation signal frequency of 10.0 kHz.

The capability of the air-water loop to achieve specific flow patterns is shown in Figure 4. The vertical flow map was used for the demonstration of the flow regimes obtained from the flow loop. The Red area presents the original working flow conditions [15], which was extended to the Blue area by the device reconfiguration [16]. Therefore, in the vertical pipe section, it is possible to generate slug, churn and annular flow patterns, also produce stratified, wavy, plug, slug and annular flow patterns in the horizontal pipe section. Figure 4 shows 10 slug and churn flow measurement points (variant 1-10) as references for 10 annular flow measurement points (variant 11-20) in the vertical pipe section. The flow conditions, including corresponding Reynolds numbers, are presented in Table 2.

3. Results and discussion

3.1. Annular flow observation

In the annular pattern, part of the liquid flows as a film along the wall and other part as drops entrained in the gas. The interfacial stress varies with the flow rate of the film. Thus, the pressure gradient depends on the fraction of the liquid flow entrained as drops in the gas. A predictive approach is to view the resulted balance between the rate of atomisation of the liquid film and the rate of deposition of drops. Thus, measurements of film are a priority. The knowledge of drop size is of importance since it is needed to predict drop turbulence and the influence of gravity on the motion of drops. The estimation of annular flow and the initiation of atomisation are based on the properties of waves at the interface measurement, the interfacial stress and the water film thickness prediction. The droplets size and behaviour in the core is not available via EIT techniques due to the low-conductive environment shielding. The concentration tomograms show the high capability

Table 2: Specification of measuring point

Sensor position, variant no.	Gas superficial velocity [m/s]	Liquid superficial velocity [m/s]	Re_{Gas} [-]	Re_{Liquid} [-]	Flow regime
1	0.1	0.11	2×10^2	4.6×10^3	Bubble / Slug
2	0.2	0.11	4×10^2	4.6×10^3	Bubble / Slug
3	0.3	0.11	6×10^2	4.6×10^3	Slug
4	0.4	0.11	8×10^2	4.6×10^3	Slug
5	0.5	0.11	1×10^3	4.6×10^3	Slug
6	0.7	0.11	1×10^3	4.6×10^3	Slug
7	0.9	0.11	2×10^3	4.6×10^3	Slug
8	2.5	0.11	5×10^3	4.6×10^3	Slug / Churn
9	5.1	0.11	1×10^4	4.6×10^3	Churn
10	7.1	0.11	1×10^4	4.6×10^3	Churn
11	10.1	0.12	2×10^4	5.0×10^3	Annular
12	11.1	0.13	2×10^4	5.8×10^3	Annular
13	12.5	0.14	2×10^4	6.3×10^3	Annular
14	13.7	0.15	2×10^4	6.4×10^3	Annular
15	15.0	0.16	3×10^4	6.6×10^3	Annular
16	16.0	0.16	3×10^4	6.6×10^3	Annular
17	17.0	0.17	3×10^4	7.1×10^3	Annular
18	17.9	0.18	3×10^4	7.5×10^3	Annular
19	18.5	0.18	4×10^4	7.5×10^3	Annular
20	19.1	0.18	4×10^4	7.5×10^3	Annular

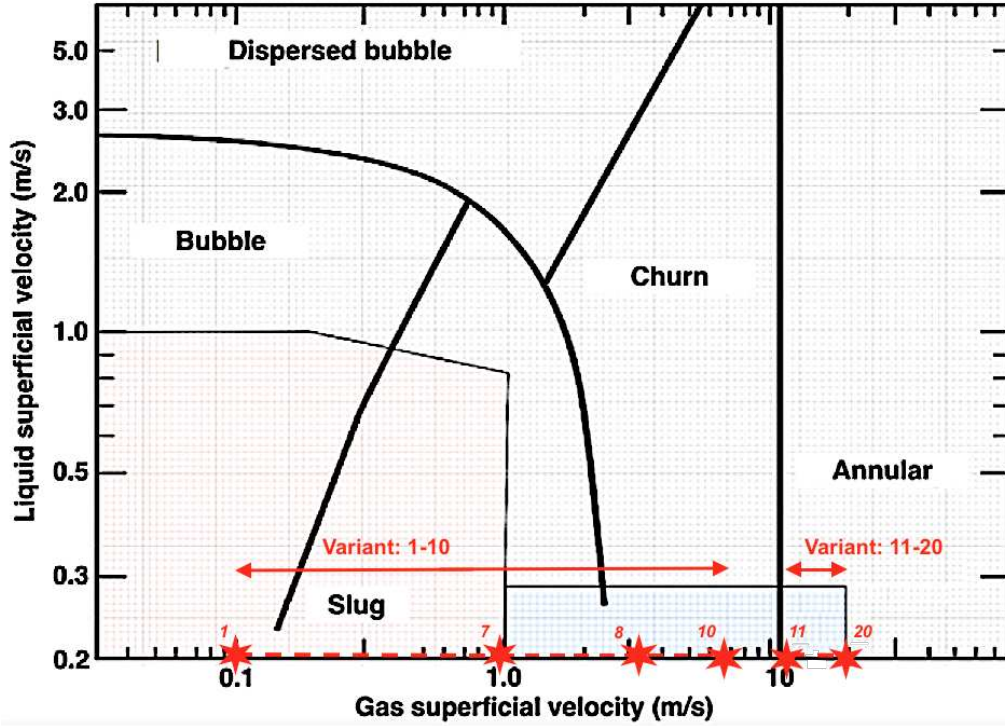


Figure 4: The working area of laboratory air-water loop, vertical flow patterns, Slug (reference) measurement points no.1-10 ($U_g = 0.1 - 1m/s$), Annular flow measurement points no.11-20 ($U_g = 10 - 19m/s$)

of water film thickness and flow instability studying. The 16 electrodes sensors are connected with the fast impedance camera system (EIT techniques) and synchronise with a slow motion camera (500 frames per second). The photography of water film demonstrates the instability at different vertical flow conditions (Figure 5), which were operated at different water velocities. The mechanism is known as Rayleigh-Taylor instabilities [17].

3.2. POD analyses

Different thermal and flow conditions can be characterised through different structure of multiphase flow dynamic behaviour. A specific mode of decomposed EIT signal can be used to represent the prevalent annular flow regime within the pipeline.

The estimation of the first dominant basic function enables, with certain probability, the estimation of the annular flow conditions based on the ac-

quired EIT measurement from gas-liquid flow. The EIT-based images are given in terms of stacked concentration tomograms presenting a vertical annular flow. Comparing with other vertical flow conditions, stacked tomograms for slug and churn flow regimes are presented in Figure 6. Figure 7 presents the original EIT tomograms of a vertical annular flow. From tomograms, several typical flow phenomena of annular flow can be identified, e.g. the liquid film, gas core consisting of tiny air bubbles, high frequency waves, oscillating liquid membrane [24] and interfacial shear waves. It is quite apparent that, the EIT technique can be utilised for validation of the results generated from the POD.

Figure 8 presents POD images reconstructed using the 3rd POD mode (relative error below 6%). The images demonstrate the extraction of flow information which characterises the EIT signal from dynamic point of view and illustrates the capability of original image reconstruction according to the extracted basic function with certain accuracy. Both attributes of POD techniques, decomposition and reconstruction, are utilised for flow regime recognition based on the developed reduce-order model [16].

Figure 8 presents POD images reconstructed using the 3rd POD mode (relative error below 6%). The images demonstrate the extraction of flow information which characterises the EIT signal from dynamic point of view and illustrates the capability of original image reconstruction according to the extracted basic function with certain accuracy. Capabilities of signal decomposition and reconstruction, are utilised for flow regime recognition based on the developed reduce-order model [16].

Within separated flows there are different scales of gradations and degrees of phase separation. The velocity difference between gas and liquid flows in a pipe, which consists of two single phase streams, can designate a fully separated flow. On the other hand, most annular flows in a vertical pipe consist of a film of liquid on the walls and a central core of gas that contains a significant number of liquid droplets (see figure 9). These droplets are an important feature of annular flow and therefore the flow can only be regarded as partially separated.

3.3. Probability density function of void fraction

Probability density of gas and liquid concentration is a function in PDF, whose value at a given measurement time interval with the EIT sensor planes can be interpreted as providing a relative likelihood. The value of the concentration would equal to measurement sample. The value of the PDF from two

different measurement samples can be used to infer actual flow conditions. The PDF allows the detail statistical analysis of dynamic aspect of EIT data as well.

The statistical analysis based on PDF consist of the following tasks:

- Decompose the EIT signal to the separate phases: pure liquid, pure gas, mixture (tiny bubbles, foam) for each pixel.
- Specify the void fraction for each phase and each snapshot (time step), see Figure 9 and 10.
- Calculate the histogram of probability density function of void fraction for whole area (all pixels) and limited areas: boundary and core zones, see zones definition on Figure 11.
- Compare the similarity of each histogram and determine probable flow regime and flow conditions.

The evolution of phase void fractions of slug and churn flow regime (Figure 9) and annular flow regime (Figure 10) according to defined zones (Figure 11) were analysed from the frequency of occurrence.

Figures 12 and 13 show the probability density function of liquid and gas void fractions of variant 1-10 (bubble, slug and churn flow) and 11-20 (annular flow). Probability densities of all phases were estimated for all pixels (the left column), boundary or pipe wall zone (the middle column) and core zone (right column). The definition of the boundary and core zones for vertical pipeline is obviously shown in Figure 12 . It is notable that the definition for horizontal pipeline should be different, for example, at the bottom, middle and top zones, to recognise the gravity effect.

The typical value of disperse phase for annular flow is below 5%, which could be neglected for this analyse. The liquid, in respect to gas void fraction, has an approximately constant value. The most frequent situation in vertical pipeline is $LVF < 20\%$, respectively $GVF > 80\%$, where LVF and GVF denote the liquid volume fraction and the gas volume fraction respectively. PDF void fraction histogram for the core zone is similar to void friction distributions at all pixels in the case of annular flow regime, because liquid is mainly located in the wall zone. The probability distribution for slug and churn flow regimes (see Figure 13) is different, where the intermittent behaviour is more uniform then the annular flow regime. Increase of Liquid

superficial velocity causes thinning of the liquid film and this corresponds to increasing of the probability of lower water concentration. Contrary, the forming of liquid membrane causes an increase of the local water layer which corresponds to increase the probability of lower liquid void fraction.

The comparison of annular flow variants shows the influence of distribution profile on gas superficial velocity. Recurrent tomographic measurements shows, the distribution profile is unique for specific flow conditions according to considerable dynamics of predominant flow instability. This fact could be used as a preliminary flow regime recognition.

3.4. Frequency analyses of POD functions

A frequency analysis of POD time functions was performed to determine the dominant frequencies of slug, churn and annular flow regime. Figure 14 shows dominant frequencies of the first three POD modes. The typical frequency of slug and churn flow regime is around 1-3 Hz. For annular flow variants there is a shift towards higher frequencies and lower amplitude. For the variants 18-20, the 5 Hz frequency is observed, which is one of the typical annular flow frequency of measured flow condition [18]. The second typical frequency, 16Hz is not apparent here probably due to the fact, there is no fully developed flow regime produced at the experimental device.

3.5. Error analyses

The accuracy of concentration image reconstruction is strongly depending on the number of POD modes. The comparisons of relative errors for 2, 3, 4 and 5 modes reconstruction are shown in Figure 15. The present relative error is average value over measuring time and domain of the ratio of absolute error of reconstructed image using specific number of POD modes to the original EIT image. The errors are calculated for 8000 frames (10s data acquisition). It is obvious, the reconstruction involving the fifth POD mode causes the reduction of the error on the half, approximately. Anomalous relative errors are reported for variants 1,2 and 8, which corresponds with transition between bubbly and slug, respectively between slug and churn flow regime.

Typical error of annular flow reconstruction is 2-3 times lower than slug and churn flow regime reconstruction. This trend corresponds with the eigenvalues ratios. The typical ratio of the first and second POD eigenvalues of slug and churn is 20 - 100 and 300 - 3000 for annular flow. Precipitous increase of the ratio for annular flow corresponds to the decrease of the higher

POD order energy signification and to related decrease of the reconstruction error. Sensitivity of the eigenvalues in respect to energy, ratio to flow regime is captureable by relative energy analyses.

3.6. Relative energy analyses

The eigenvalues calculated within POD analyses reflect the relative energy of the specific POD mode. Specific eigenvalues composition corresponds with specific flow regimes, showing from the first five eigenvalues in Figure 16. It is apparent that increasing the magnitude of first mode resulted in decreasing the magnitude of high order modes for annular flow. The typical first eigenvalues magnitude of the slug flow reflect 80% of total energy, which is usually more than 98% for annular flow.

3.7. Potential coupling of POD with Wavelet analysis

In addition to POD, Wavelet analysis is also a suitable technique for multiphase flow pattern characterisation and recognition [19]. Both methods are capable to reconstruct and analyse multiphase flow field in terms of fluctuating energy and time frequency distribution. From literature [20], it is apparent that the first few wavelet components and POD modes can give the representation of the most energetic structure at large scales, in respect to the total fluctuating energy. Both methods are used as a reduced-order models (ROMs) as well. In the ROMs the large amount of experimental data are replaced by a much smaller number of coefficients of ordinary differential equations [21].

The POD allows the overall view of the most energetic flow pattern in a domain by decomposing the multiphase flow field in to spatial and temporal modes, while wavelet transform gives the localised spatial information through scale wise decomposition of the flow field. There are known studies that apply the wavelet transform on the POD spatial modes [22]. That combination allows understanding of the space scale structure of the flow events captured by the spatial POD modes, which relates to the specific and energetic flow events over period of time with the localised dominant scales that contribute to it.

Another alternative technique for multiphase flow regime characterisation is based on multivariate and multiscale Entropy analysis [23]. The study presents multivariate multiscale Entropy sensitivity to the change of flow velocity. The flow pattern transition can be detected by those changes on a different scale.

4. Conclusion

The aim of this paper is to implement the proper orthogonal decomposition method supplemented by frequency and statistical EIT signal analyses as a post-processing technique for vertical annular flow pattern characterisation. The result shows that the unique fluid dynamic behaviour of specific flow regime and specific flow transition can be detected by present post-processing method. This fact is well demonstrated on frequency analysis of POD modes, error analysis of POD image reconstruction and probability density function of void fraction for specific zones. The introduced method decomposed the EIT signal to the certain number of POD modes, which each one corresponds to specific flow phenomena. Frequency analyses of POD modes, instead of full signal analyses, identify the frequency of typical flow instabilities of specific flow regime.

The relative error of the signal reconstruction strongly relates to flow conditions and order of POD modes. The error of annular flow reconstruction is typically twice lower than that of slug flow reconstruction, reducing with gas superficial velocity increasing. The transitions of bubbly, slug and churn were captured clearly by anomalous error increasing for variants 1,2 and 8.

Probability density function of void fraction could be simple and fast preliminary standard for flow regime estimation. More than the appropriate distribution profile, the ratio between specific zones is important. The comparison could detect the differences of intermittent flow behaviour between the core and boundary of vertical pipeline, respectively the bottom and top of horizontal pipeline. These differences are unique for specific multiphase flow regime.

5. Acknowledgement

This research was supported by European Association of National Metrology Institutes, project ENG58, Multiphase flow metrology in oil and gas production.

6. References

- [1] F. A. Holland, R. Bragg, Fluid Flow for Chemical Engineers. London : Edward Arnold, (1995) 219-267

- [2] D. Lavicka, J. Polansky, Model of the cooling of a nuclear reactor fuel rod, *Multiphase Science and Technology*, DOI: 10.1615, *MultScienTechn.v25.i2-4.90*, (2013) 237-248
- [3] C.E. Brenner, *Fundamentals of Multiphase Flows*, California Institute of Technology Pasadena, Cambridge University Press, (2005) ISBN 0521 848040
- [4] D. Baker, Simultaneous Flow of Oil and Gas, *Oil and Gas J*, 53, (1954) 183-195
- [5] G.F. Hewitt, D.N. Roberyson, *Studies of Two-Phase Flow Patterns by Simultaneous X-ray and Flash Photography*, Rept AERE-M2159, UKAEA, Harwell (1969)
- [6] E.W. Jassim, T.A. Newell, J.C. CHato , Probabilistic Flow Regime Map Modelling of Two-phase flow. Illinois : University of Illinois, (2006) 1-6
- [7] V. Bertola , *Modelling and experimentation in Two-Phase Flow*, Springer-Verlag Wien New York (2003), ISBN 978-3-211-20757-4
- [8] C. Kleinstreuer, *Two-Phase Flow: Theory and Application*. New York (2003), Taylor and Francis, 69-75.
- [9] M. Wang, *Industrial Tomography, Systems and Applications*, ISBN 978-1-78242-123-8, Elsevier (2015)
- [10] J. L. Lumley. The structure of inhomogeneous turbulent flows. In *Atmospheric Turbulence and Radio Wave Propagation* (ed. A. M. Yaglom & V. I. Tartarsky), p. 166. Nauka, Moscow (1967)
- [11] J.P. Bonnet, D.R. Cole, Stochastic Estimation and proper orthogonal decomposition: Complementary techniques for identifying structure, *Experiments in Fluid* 17 (1994)
- [12] S. Volkwein, *Proper Orthogonal Decomposition: Theory and Reduced-Order Modelling*, University of Konstanz, lecture note, (2013)
- [13] C. Laurent, M. Bergman, Post-processing of experimental and numerical data, POD: an overview, von Karman Institute for Fluid Dynamics, Lecture Series, (2003)

- [14] B.A. Belson, J.H. TU ,C.W. Rowley , A parallelized model reduction library, Princeton University, (2013)
- [15] N.P. Ramskill, M. Wang , Measurement and recognition of gas-liquid multiphase horizontal flow regimes using electrical resistance tomography in: 6th World Congress in Industrial Process Tomography, (2010) 159-167
- [16] J. Polansky, M. Wang, Proper Orthogonal Decomposition as a technique for identifying two-phase flow pattern based on electrical impedance tomography, Flow Measurement and Instrumentation, Volume 53, Part A, (2017) Pages 126132
- [17] G. Yadigaroglu, Instabilities in two-phase flow, Swiss Federal Institute of Technology, Zurich, 2015
- [18] G.F. Hewitt, N. S. Halle-Taylor , Annular Two-Phase Flow, ISBN, 0080157971, New York Pergamon Press, (1970)
- [19] Ch. Tan, P. Li, W. Dai, F. Dong, Characterization of oilwater two-phase pipe flow with a combined conductivity/capacitance sensor and wavelet analysis, Chemical Engineering Science 134, (2015) 153168
- [20] S. Gordeyev, POD,LSE and Wavelet decomposition: Literature Review, University of Notre dame
- [21] T.A. Brenner, Practical Aspects of the Implementation of Reduced-Order Models Based on Proper Orthogonal Decomposition Texas A&M University, PhD theses, (2011)
- [22] V.T. Mandar, J.S. Mayur, S.D. Sagar, B.J. Jyeshtharaj, A hybridized snapshot proper orthogonal decomposition-discrete wavelet transform technique for the analysis of flows tructures and their time evolution, Chemical Engineering Science 64, (2009) 4319-4340
- [23] Ch. Tan, J. Zhao, F. Dong, Gaswater two-phase flow characterization with Electrical Resistance Tomography and Multivariate Multiscale Entropy analysis, ISA Transactions 55, (2015) 241249
- [24] T. J. Handratty, Physics of Gas-Liquid Flows, University of Illinois at Urbana-Champaign, ISBN 978-1-107-04120-2, (2013)



Figure 5: Photography of vertical annular flow, variant 10 (left), 15 (middle) and 20 (right), water film instability as a function of gas superficial velocity

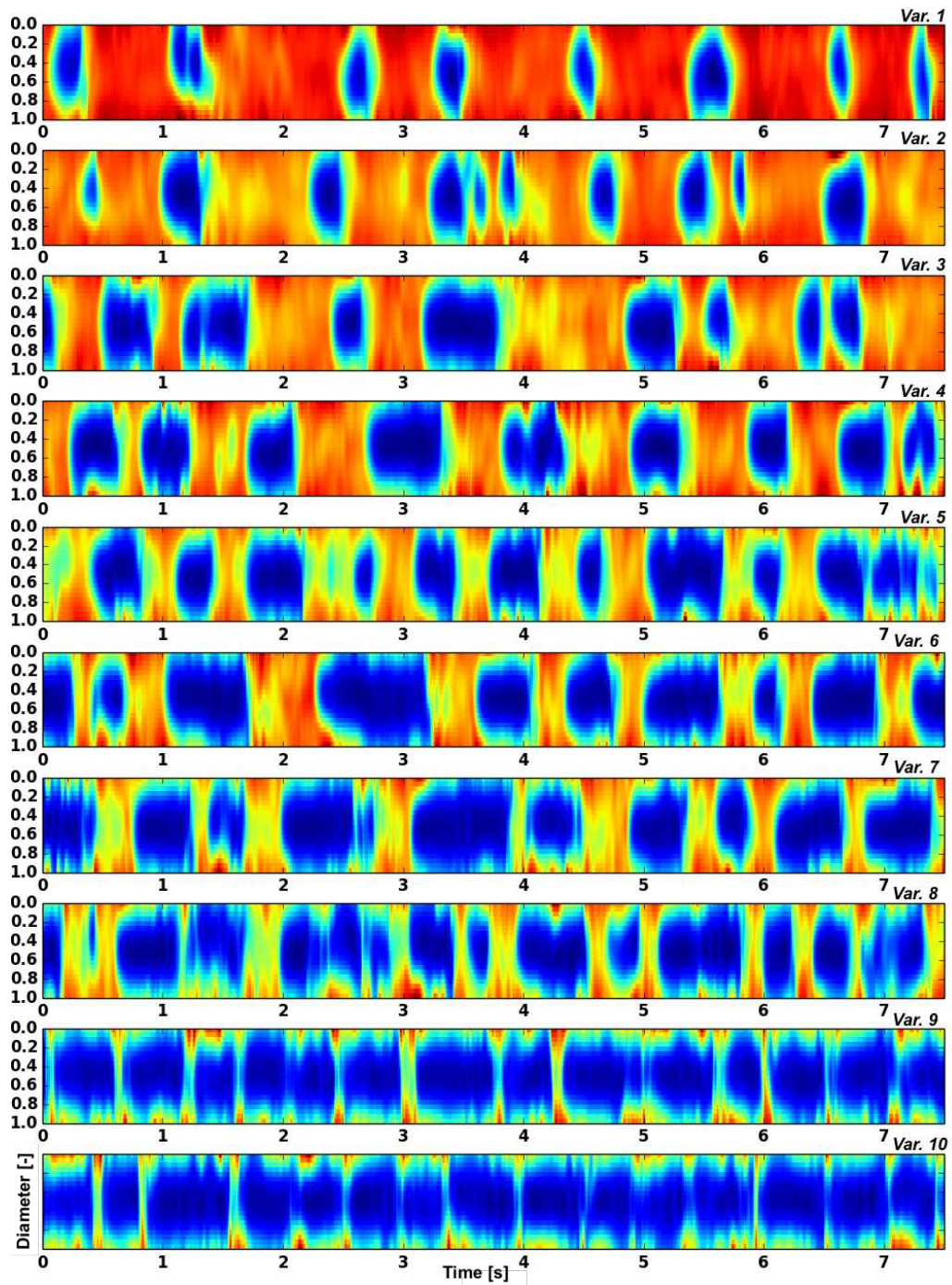


Figure 6: Stacked concentration tomograms of vertical slug flow (variant no. 1 - 10), original EIT image

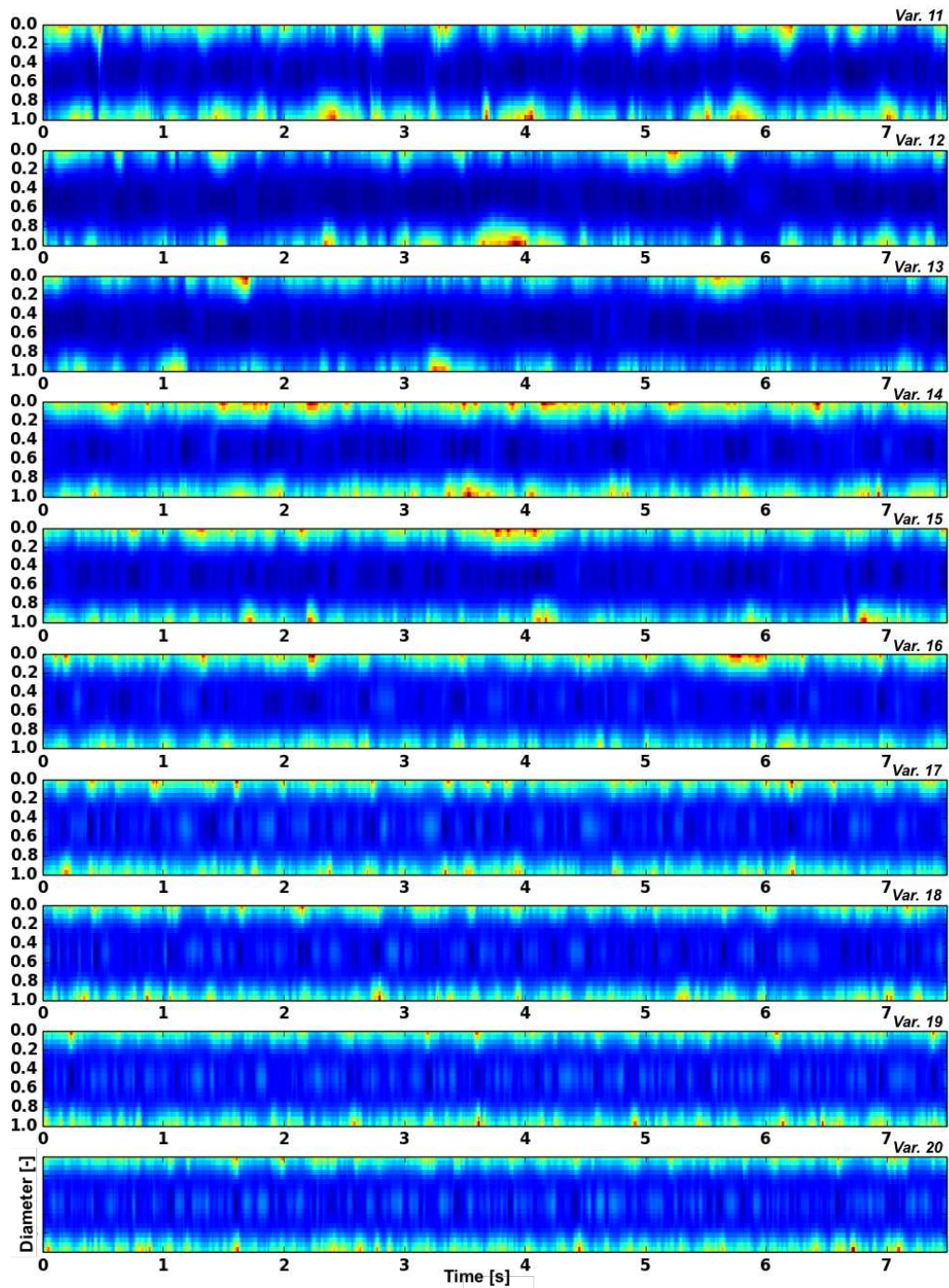


Figure 7: Stacked concentration tomograms of vertical annular flow (variant no. 11 - 20), original EIT image

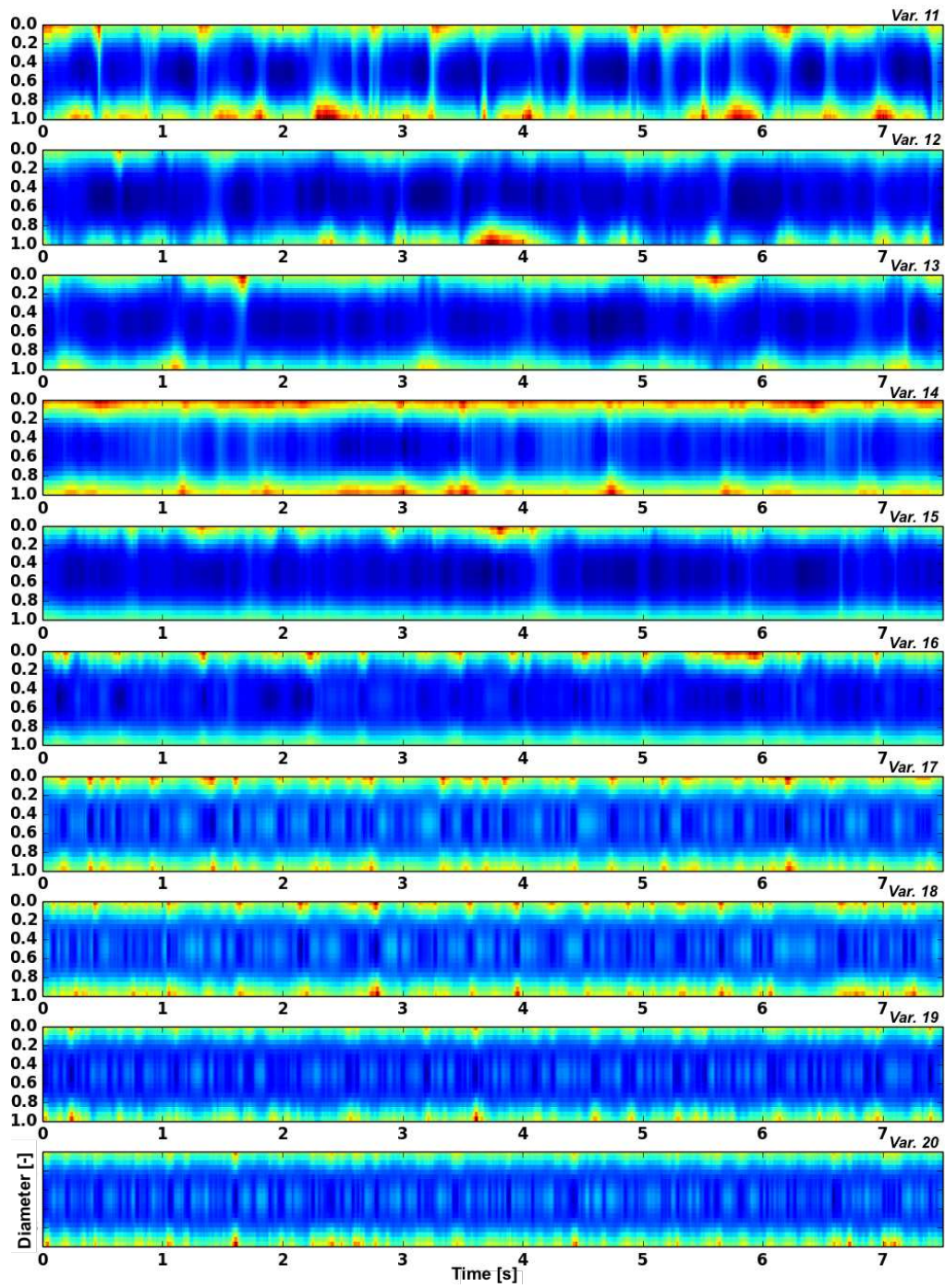


Figure 8: Stacked concentration tomograms of vertical annular flow (variant no. 11 - 20), 3rd POD mode reconstruction

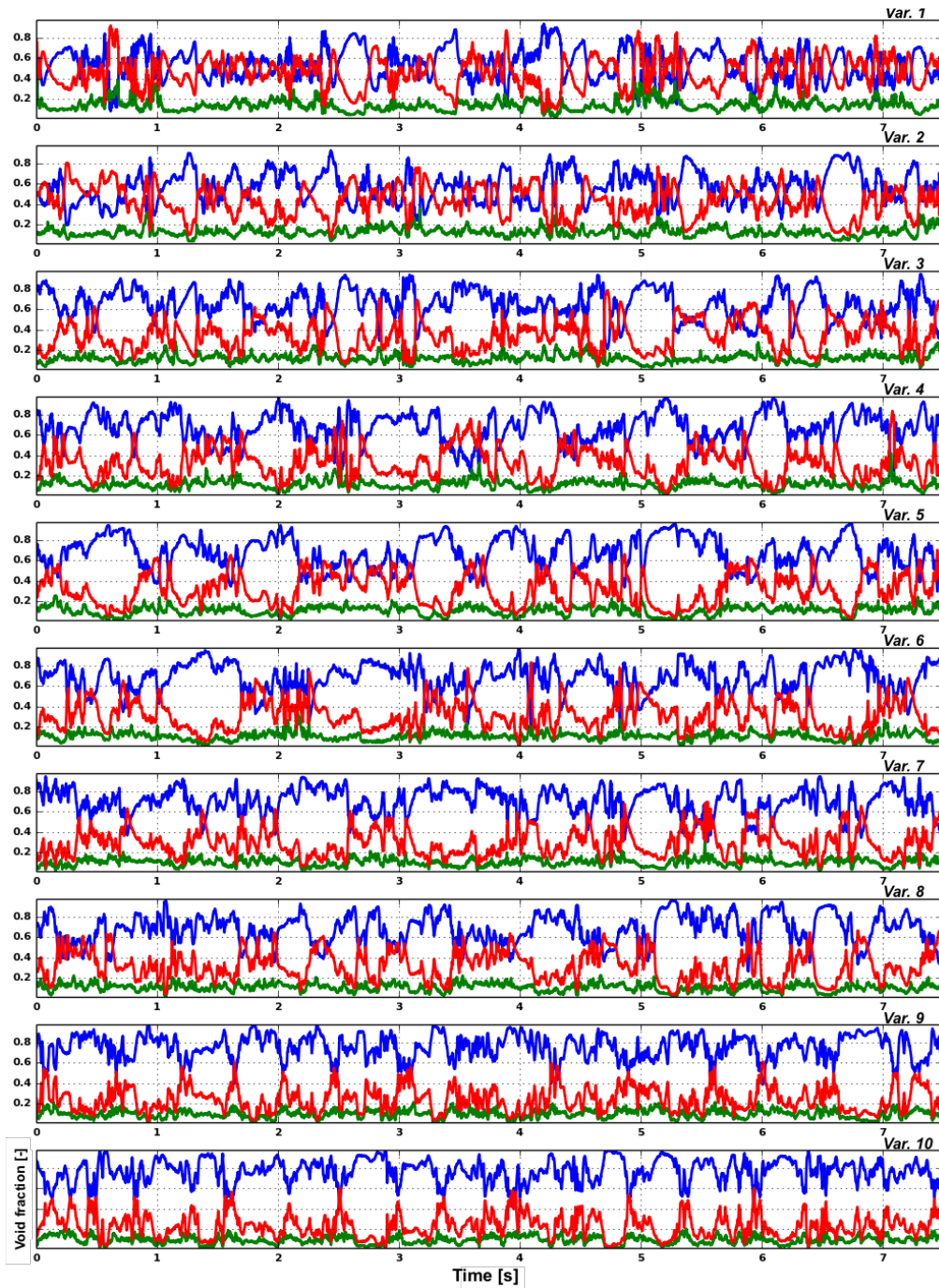


Figure 9: Void fraction of liquid (red), gas (blue) and disperse phase (green), slug flow regime, variant no. 1 - 10

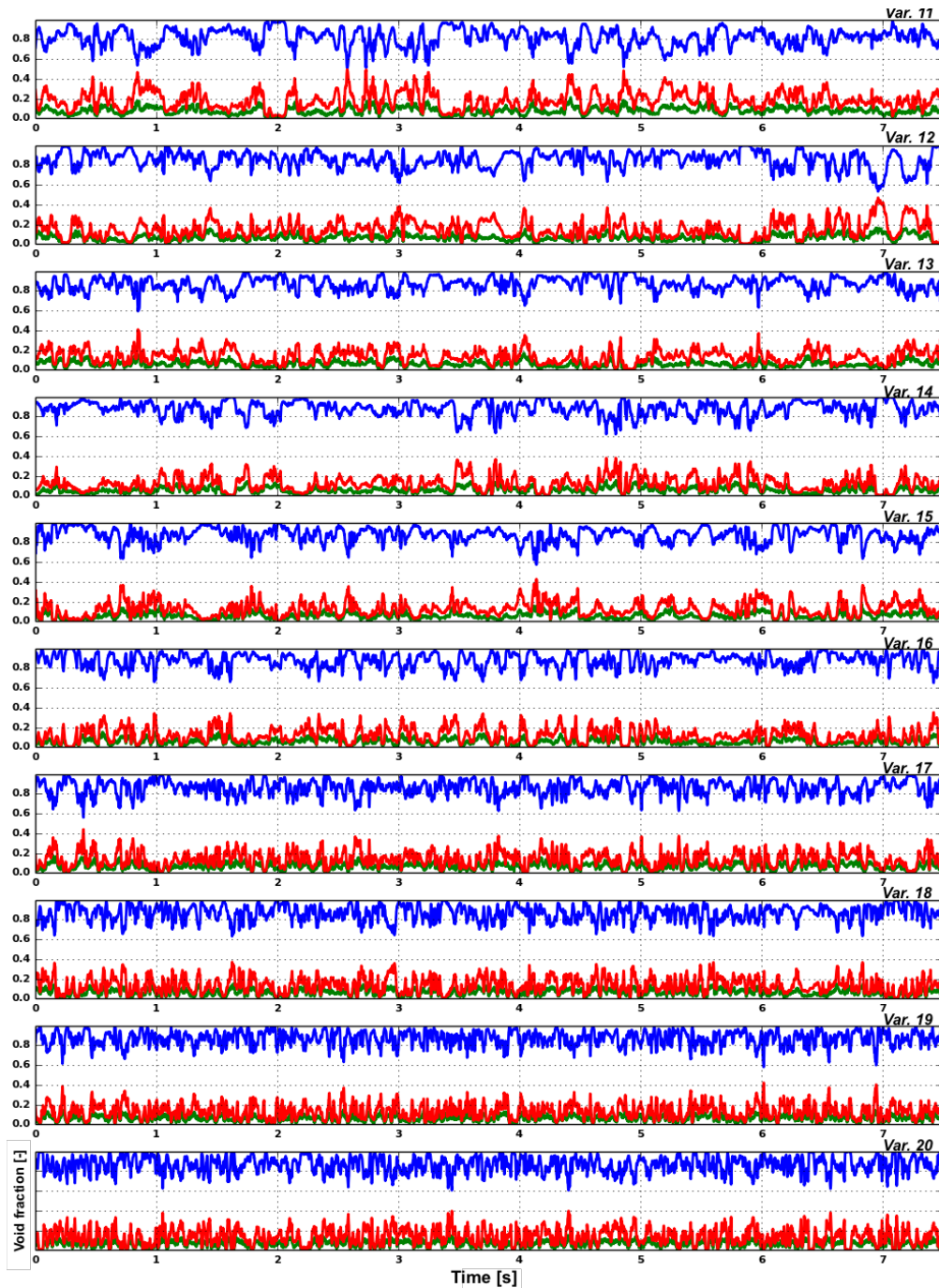


Figure 10: Void fraction of liquid (read), gas (blue) and disperse phase (green), annular flow regime, variant no. 11 - 20

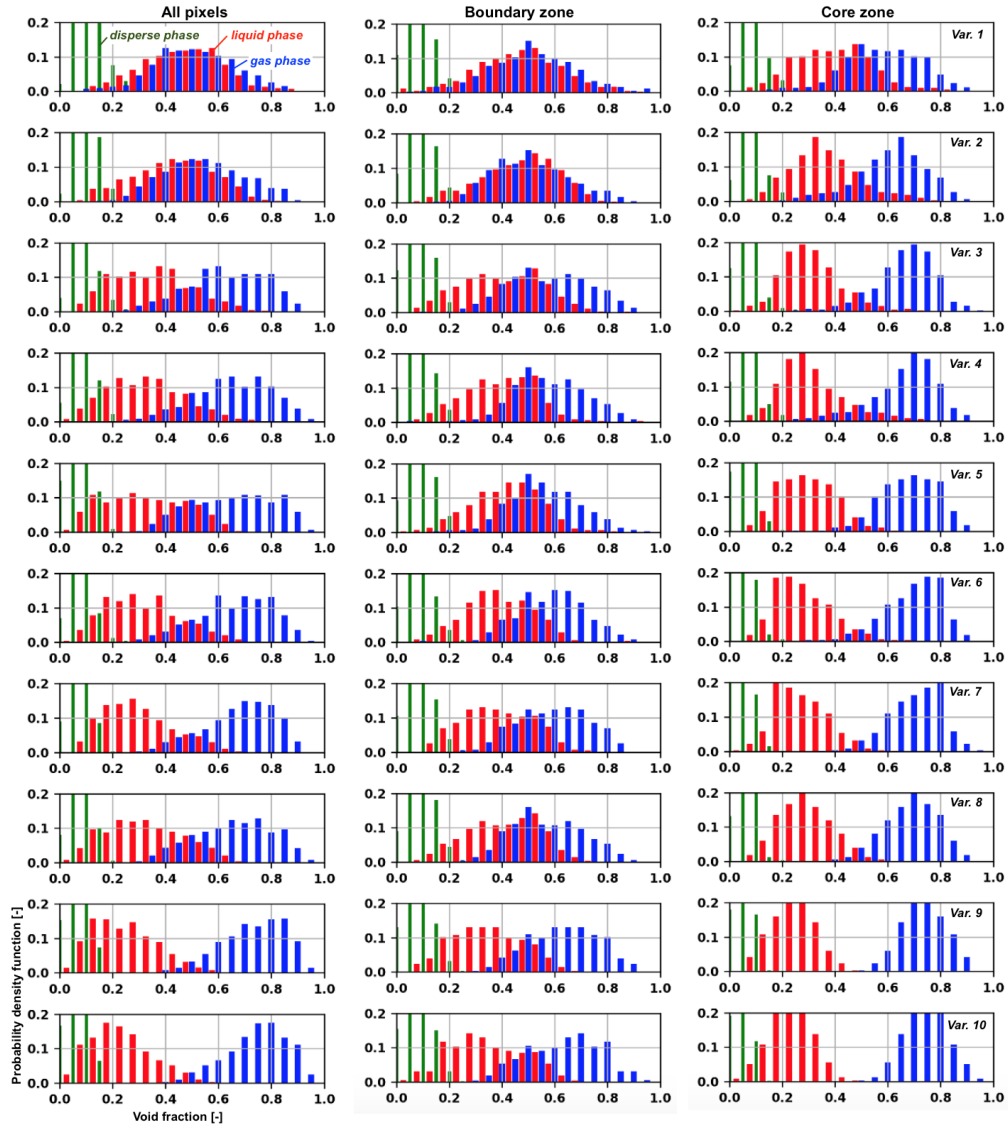


Figure 12: Probability density function of void fraction, all pixels (left), boundary zone (middle), Core zone (right), slug flow regime, variant no. 1 - 10

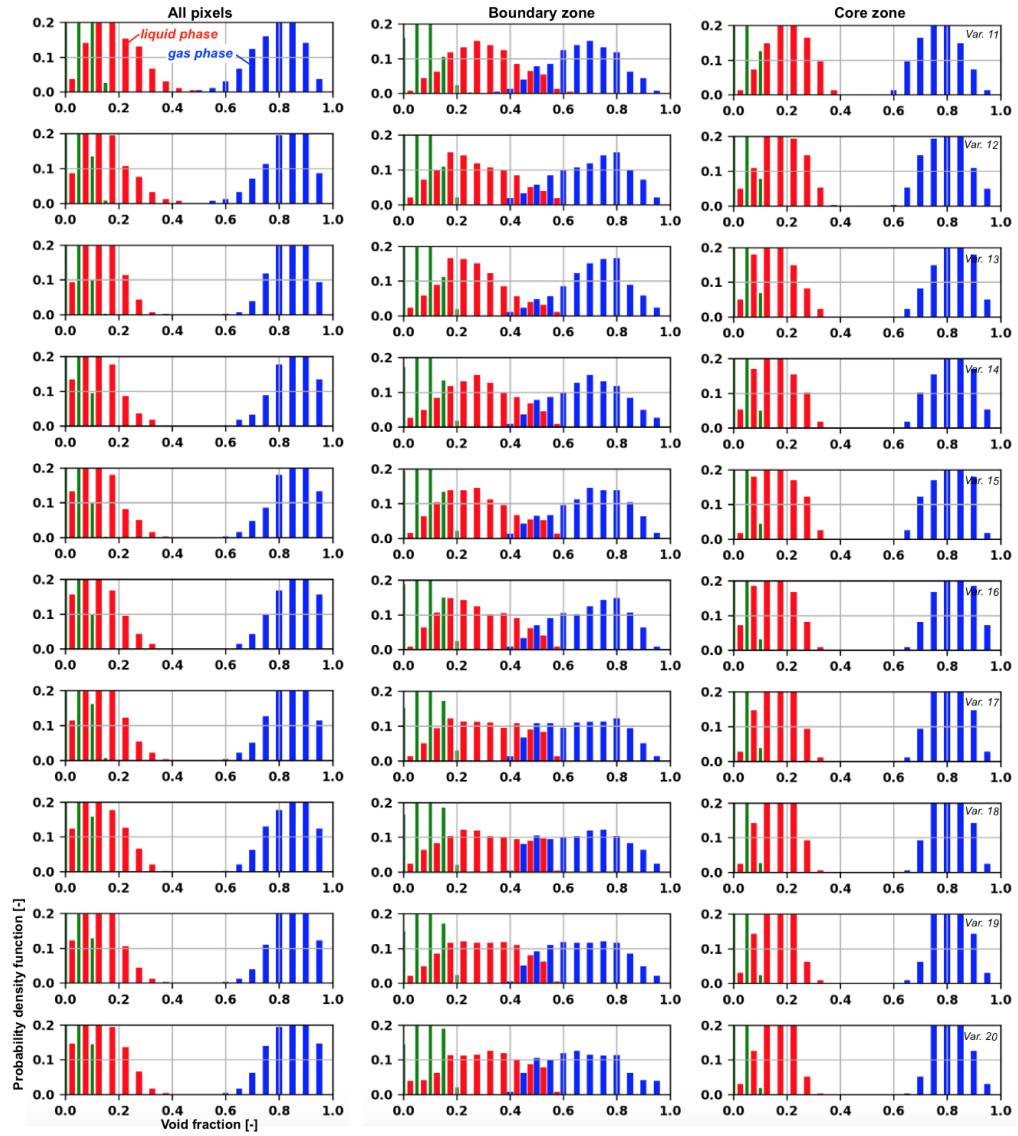


Figure 13: Probability density function of void fraction, all pixels (left), boundary zone (middle), Core zone (right), annular flow regime, variant no. 11 - 20

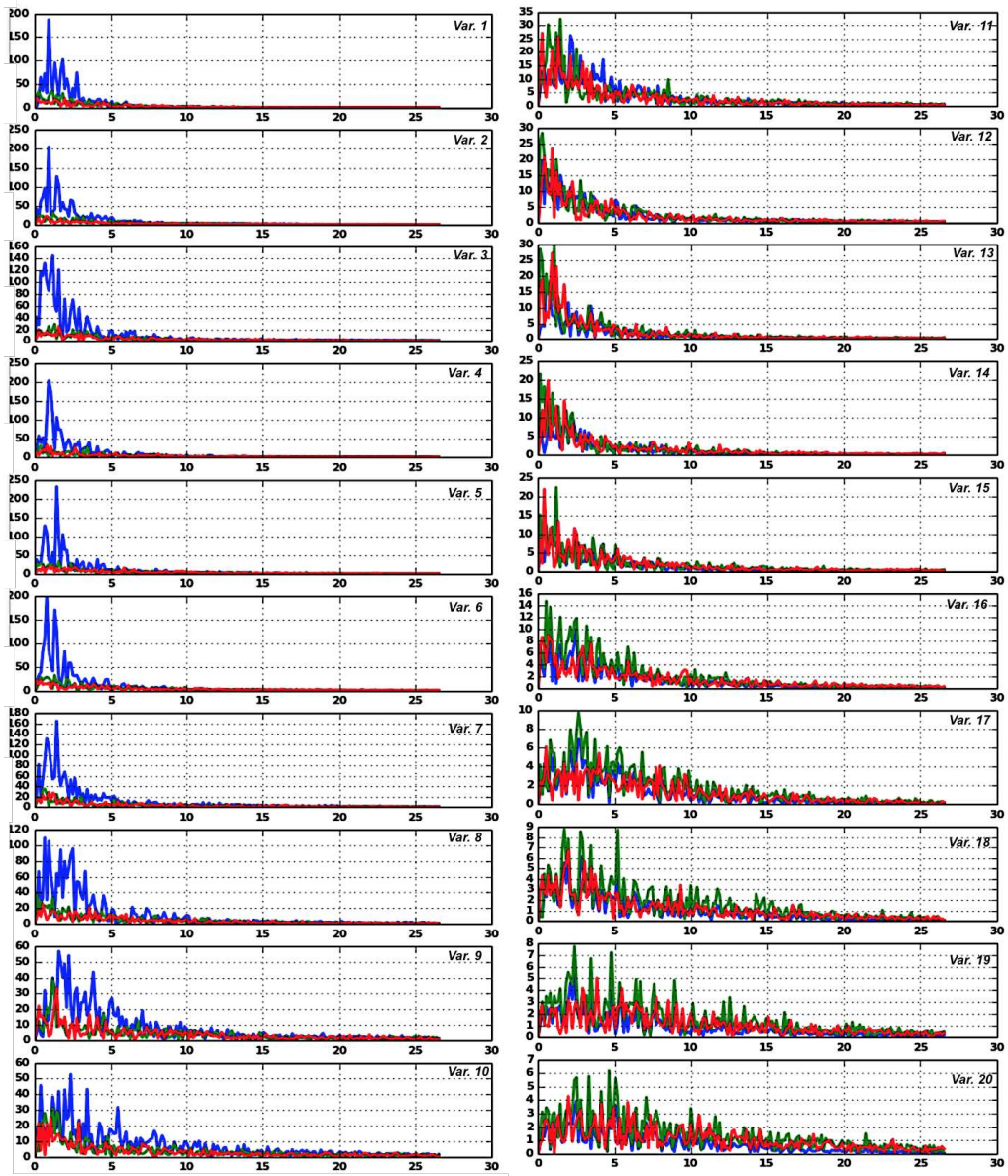


Figure 14: Frequency analysis of POD time function

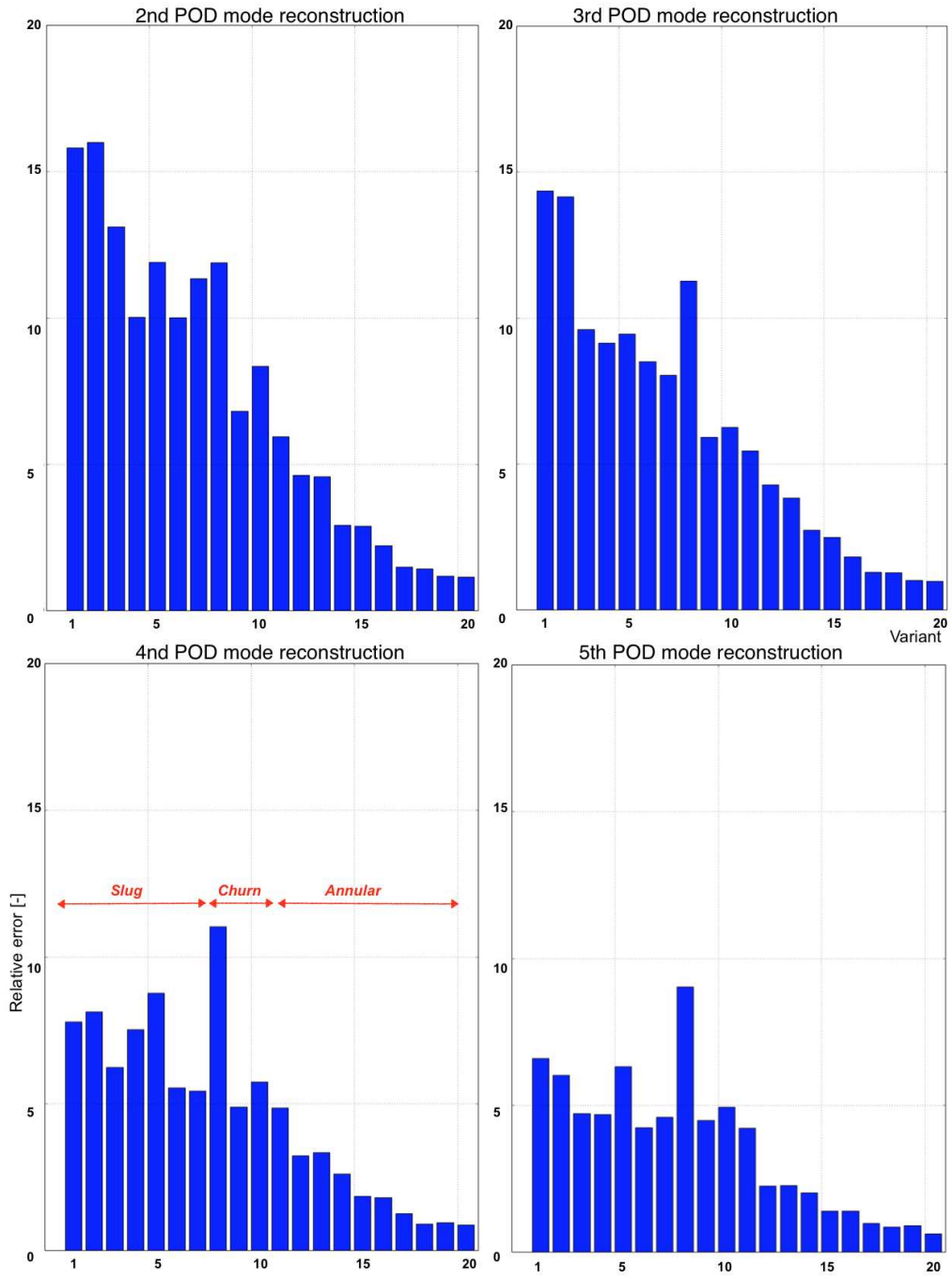


Figure 15: Relative error of POD reconstruction as a function of order of POD modes

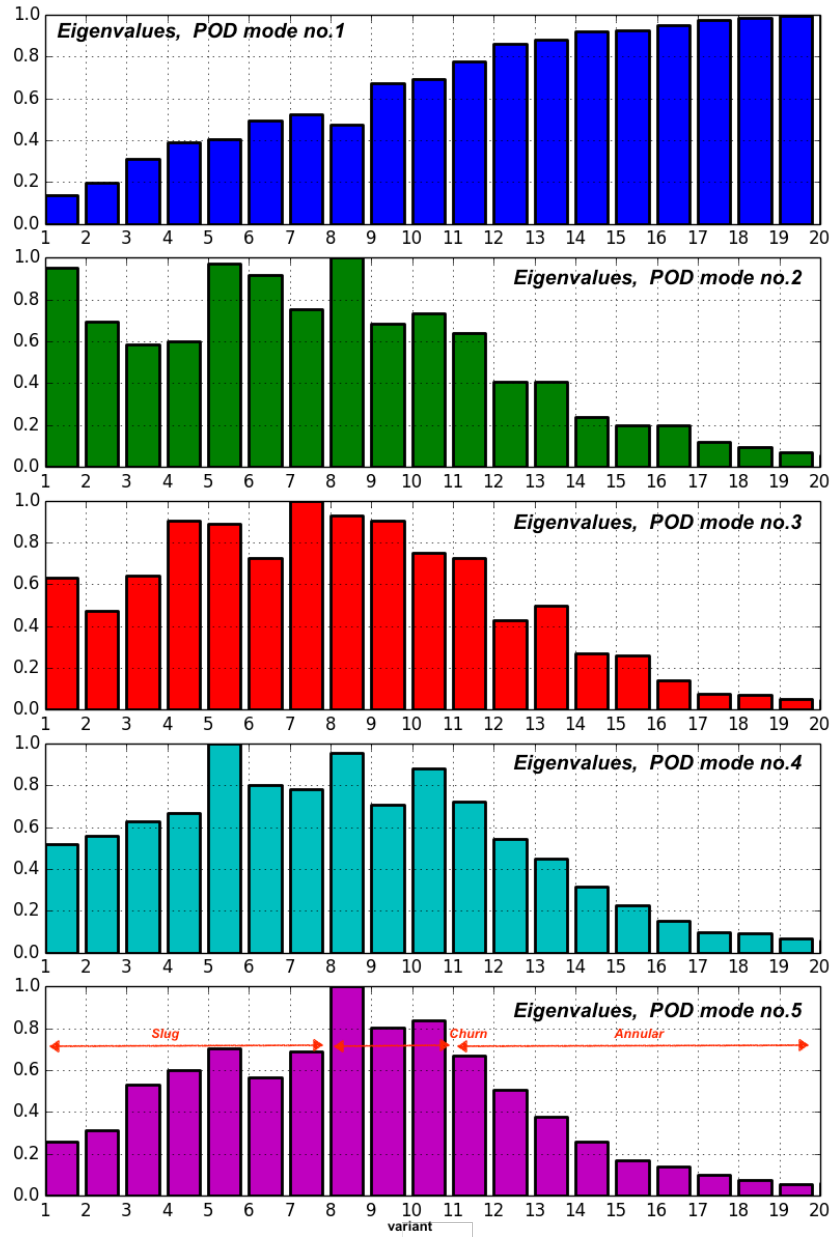


Figure 16: Normalised eigenvalues of 1st to 5th POD modes